1in

Investigation into surface roughness characterisation using LiDAR and cameras

---

Presented by:

Agoritsa Spirakis

Prepared for:

Robyn Verrinder and James Hepworth

October 13, 2025

Submitted to the Department of Electrical Engineering at the University of Cape Town in partial fulfilment of the academic requirements for the degree of BSc Eng Electrical and Computer Engineering.

Abstract

This thesis investigates the use of LiDAR and camera technology for the purpose of characterization of surface roughness. The application of this research is to eventually be used to characterize sea ice in the Marginal Ice Zone near Antarctica. This would assist in understanding the dynamics of the sea ice due to the effect surface roughness has on the drift of sea ice. This research provides a preliminary investigation by analyzing current literature in surface roughness characterization of sea ice and optimal point cloud processing algorithms. A point cloud dataset is gathered from the Velodyne VLP-16 on the Clearpath Husky UGV through rigorously designed experiments using 3D printed surfaces of known roughness. The data collected provides a set of varied position parameters in the X, Y and Z directions through the manipulation of external experiment parameters. A point cloud processing pipeline is suggested and the preprocessing of this methodology is demonstrated in MATLAB. The plane extraction uses the robust RANSAC Algorithm the positional relationship between physical and point cloud measurements is done using the Iterative Closest Point Algorithm (ICP). This methodology yielded a good model from the point cloud data with the best results at distance less than 1m.

Acknowledgments

I would like to thank my two amazing supervisors, Miss Robyn Verrinder and Mr James Hepworth.

I would also like to thank Mr Justin Pead and Mr Brendon Daniels for the assistance with my 3D printing and Dr Paul Amayo for entrusting with the Husky robot for my experiments.

This project would not have been possible without the incredible support from my parents, my boyfriend, my friends and my two sausage dogs.

Plagiarism Declaration

1. I know that plagiarism is wrong. Plagiarism is to use another's work and pretend that it is one's own.

2. I have the IEEE convention for citation and referencing. Each contribution to, and quotation in, this final year project report from the work(s) of other people, has been attributed and has been cited and referenced.

3. This final year project report is my own work.

4. I have not allowed, and will not allow, anyone to copy my work with the intention of passing it off as there own work or part thereof.

.....

Agoritsa Spirakis

October 13, 2025

Contents

List of Figures

List of Tables

Chapter 1

Introduction

1.1 Introduction

Currently, the earth is experiencing unprecedented climate change so the analysis of the sea ice in the Antarctic region would prove valuable in the efforts to monitor and combat this change in climate. Ice formation is affected by several interacting forces including local wind and wave conditions. In particular, the surface roughness of ice influences the sea ice dynamics.

1.2 Motivation

This research contributes a preliminary investigation into sea ice roughness characterization. It forms part of UCT's Marine and Antarctic Research for Innovation and Sustainability (MARIS) research group, an interdisciplinary unit focused on the development of technological and innovative solutions for complex marine problems.

1.3 Problem Statement

The distribution of sea ice in the Marginal Ice Zone in the Southern Ocean has a significant effect on global climate patterns. The ice life cycle is poorly characterized due to lack of consistent seasonal measurements in this area. A potential method for these surface roughness characterizations is using a LiDAR system. Before the system is implemented, an investigation into the collection of known surface roughness data using LiDAR will need to take place to further understand and interpret the data that will be collected from ice floe samples.

1.4 Objectives

This thesis serves as a preliminary investigation to using LiDAR technology to assess surface roughness.

Research

Exploration of literature in the field of remote sensing of earth observations, with a focus on sea ice characterization. Additionally, an investigation into surface roughness measurement and LiDAR technology.

Experiment

Collecting and analyzing a point cloud data obtained from LiDAR scans.

- Collecting a comprehensive dataset of LiDAR scans of known surface roughness.
- The effect of varying the distance between the surface and the scanner (point cloud density)

- Preprocessing analysis to the process of defining how well different shapes are characterized by the LiDAR
- Processing methodology best suited to extrapolating important surface roughness characteristics.

1.5 Thesis Contributions

The main contributions of this thesis are providing a better understanding into the use of LiDAR technology as a method to characterize surface roughness. The thesis involves a rigorous experiment design to collect a variety of data of surfaces with uniform surface roughness. This also involves the designing of these surfaces. Additionally, it provides a preliminary investigation into the LiDAR technology uses, specifically that of the VLP-16.

1.6 Terms of Reference

This section is extracted directly from the topic brief given.

1.6.1 Description

Background to the project: The distribution of sea ice in the Marginal Ice Zone (MIZ) in the Southern Ocean (SO) has a significant effect on global climate patterns, but our understanding of ice life cycle in this unique region suffers from a lack of Antarctic seasonal in situ measurement data, especially over the winter season. A variety of interacting forces, including local wind and wave conditions, strongly affect the formation and development of sea ice in the MIZ. Physical parameters such as surface roughness of Antarctic sea ice are poorly characterised, but have a marked effect on sea ice/wind/water dynamic interactions in this region. Additionally, surface

roughness influences satellite based microwave scattering measurements which are the primary mechanisms for determining sea ice coverage. Recent work by (Landy et al., 2015) has demonstrated how terrestrial based LiDAR can be used to obtain centimetre level surface roughness measurements of various sea ice types.

1.6.2 Subject of investigation

This project forms the preliminary investigation for implementing a LiDAR/camera system which will be used to characterise surface roughness of retrieved ice floes during missions. Point cloud data will be used to characterise the surface roughness of simulated surfaces, which will inform our understanding of drag effects which influence ice drift and dynamics.

1.6.3 Objectives

Objectives: The main objectives of this project are:

- Understand the requirements of the project
- Conduct a literature review of previous work in this field and critically evaluate current technology/research
- Design a series of experiments which use 3D LiDAR and cameras to take measurements of surfaces of varying levels of roughness and design the algorithms to process these data
- Test and evaluate the system performance based on a performance metrics
- Discuss the performance of the system, draw conclusions and make recommendations for future improvements

1.6.4 Deliverables

- A literature review report and detailed project statement and plan (Hand-in 2 weeks from the initiation of the project)
- Weekly reporting of project progress and plans to the supervisor through an agreed upon communication platform,which could include online meetings
- A research project report, following the Department of Electrical Engineering Final Year Project report guidelines
- Satisfactory completion of all Engineering Council of South Africa's Graduate Attributes (ECSA GAs)
- Poster summarising the research project report

1.6.5 Skills/requirements

Strong mathematical and programming skills for the algorithm development. MATLAB/Octave or OpenCV skills for simulation.

1.6.6 GA 1: Problem Solving

LiDAR/Camera sensing for these types of measurements is non-trivial and the student will need to design a series of controlled experiments to solve this.

1.6.7 GA 4: Independent Experiment Analysis

The student will need to simulate and test the complete system under a variety of operating conditions. These experiments must be rigorously designed and carefully conducted. Experimental protocols must be noted. These experiments must

be reproducible. Experimental data must be recorded alongside metadata in a retrievable format and must be linked to the report. These data must be analysed and summarised and suitable conclusions drawn

1.6.8 Extra information

Co-supervised by: J. Hepworth

SCALE Experiment website

J. C. Landy, D. Isleifson, A. S. Komarov, and D. G. Barber. Parameterization of centimeter-scale sea ice Surface roughness using terrestrial LiDAR.IEEE Transactions on Geoscience and Remote Sensing, 53(3):1271–1286, 2015.

C. L. Parkinson. Southern Ocean sea ice and its wider linkages: insights revealed from models and observations.Antarctic Science, 16(4):387–400, 2004

M. C. Kennicutt II, et al. Sustained Antarctic research: A 21st century imperative.One Earth, 1(1):95–113, 2019

1.6.9 Area

Signal processing, image processing, fluid dynamics. Suitable for ME or EC.

1.7 Scope and Limitations

The problem statement lends itself to a large scope given that LiDAR readings are affected by a multitude of factors. This project has been restricted to investigating the surface roughness values extracted from height values obtained from point cloud readings of objects of known roughness. This work does not explore the effect of

changes in refractive index nor the readings of surfaces with unknown roughness values.

The equipment used for the experiments was limited to the instruments that UCT has in their possession as these devices carry a significant cost. The choice of LiDAR device was limited to the Velodyne VLP-16 attached to the Husky Robot. As such, this device has a limited accuracy resolution. This constraint does not hinder the processing objective as the output is still a point cloud, but perhaps not as fine roughness values can be detected.

1.8 Thesis Outline

The remainder of this thesis is organized as follows:

Chapter 2, Background: Background and literature review

Chapter 3, Methodology: Project methodology overview

Chapter 4, Design: Design and development

Chapter 5, Results: Experimental results

Chapter 6, Conclusions: Conclusions and future work

Chapter 2

Literature Review

2.1 Literature Review

2.1.1 Background

Law of Reflection

The Law of Reflection states that the angle of the incidence ray is equal to that of the reflective ray for a fully reflective surface. [1]

$$\theta_r = \theta_i \tag{2.1}$$

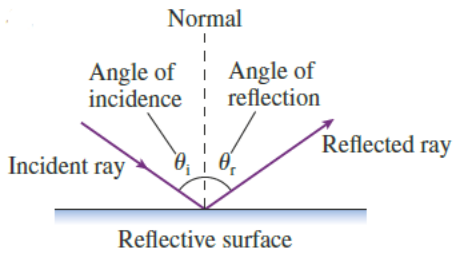

Figure 2.1: Law of reflection [1]

Diffuse Reflection

A rough surface obeys the law of reflection at every point. This results in a random scattering of the reflected rays called diffuse reflection.

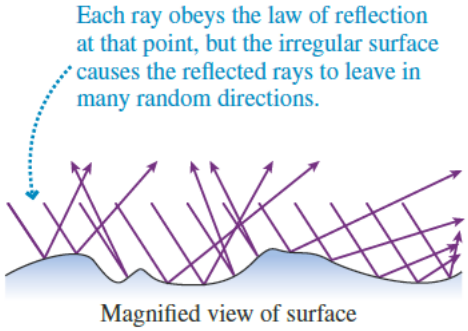

Figure 2.2: Diffuse Reflection [1]

Index of refraction

A substance's reflectively is determined by its index of refraction. The refractive index is defined as the ratio of the speed of light in a vacuum to the speed of light in the medium as shown by the equation below. [1]

$$n = \frac{c}{v_{medium}} \tag{2.2}$$

The index of refraction is used to form Snell's Law which defines effect of a light ray moving from one medium to another. [2]

$$n_1 sin\theta_1 = n_2 sin\theta_2 \tag{2.3}$$

This relationship is used in LiDAR devices to accurately gather information on the reflected light received by the device.

Scattering

The scattering of the light can either be elastic or inelastic. Elastic scattering occurs when the scattering frequency is equal to the frequency of the incidence light [3].

2.1.2 Surface roughness definition

Surface roughness can be defined in many ways. Landy describes surface roughness as deviations in surface height measured from a reference point which can be modelled as a single-scale random process. There is a group of international standards named ISO 25178 Surface Texture which describe the analysis of surface roughness. [4]

Height parameters

Height parameters: height (displacement) of the evaluation area

Category	Parameter	Description	Notes
Height parameters	Sq	Root mean square height	This parameter corresponds to the standard deviation of distance from the mean plane. It is equivalent to the standard deviation of heights.
	Ssk	Skewness	This parameter represents the symmetry of height distribution.
	Sku	Kurtosis	This parameter represents the kurtosis of height distribution.
	Sp	Maximum peak height	This parameter represents the maximum value of height from the mean plane of the surface.
	Sv	Maximum pit height	This is the absolute minimum value of height from the mean plane of the surface.
	Sz	Maximum height	This parameter represents the distance between the highest point and the lowest point on the surface.
	Sa	Arithmetical mean height	This is the arithmetic mean of the absolute value of the height from the mean plane of the surface.

Figure 2.3: Height parameters [1]

Spatial parameters

Spatial parameters: focus on the direction of the plane (wavelength direction)

Category	Parameter	Description	Notes
Spatial parameters	Sal	Auto-correlation length	This parameter represents the horizontal distance in the direction in which the auto-correlation function decays to the value[s] (0.2 by default) the fastest.
	Str	Texture aspect ratio	This parameter is a measure of uniformity of the surface texture. The value is obtained by dividing the horizontal distance in the direction in which the auto-correlation function decays to the value[s] (0.2 by default) the fastest (equivalent to Sal) by the horizontal distance in the direction of the slowest decay of auto-correlation function to the value[s].
	Std*	Texture direction	This value[s] is the angle with which the angular spectrum fAPS(S) is the largest. It represents the lay of the surface texture.

* Std, the texture direction, is classified in miscellaneous parameters in ISO 25178-2; 2012 (Surface texture parameters).

Figure 2.4: Spatial parameters [1]

Hybrid parameters

Hybrid parameters: both the height direction and the direction of the plane (wavelength direction).

Category	Parameter	Description	Notes
Hybrid parameters	Sdq	Root mean square gradient	This parameter is calculated as a root mean square of slopes at all points in the definition area.
	Sdr	Developed interfacial area ratio	This parameter is expressed as the percentage of the definition area's additional surface area contributed by the texture as compared to the planar definition area.

Figure 2.5: Hybrid parameters [1]

Other parameters

- Functional parameters: areal material ratio (bearing area) curve. They are utilized to evaluate the behavior of a surface that comes into strong mechanical contact
- Functional volume parameters: concern volumes that are calculated using the areal material ratio curve.They are utilized to evaluate the behavior of a surface that comes into strong mechanical contact.
- Feature parameters: calculated from results of peak and valley regions, respectively, segmented from the scale-limited surface

The parameters used in the research explored mainly concern height parameters, spatial parameters and hybrid parameters. The research focused on the analysis and measurement of natural surfaces, so the functional parameters were not needed as they did not study the contact mechanics of the interactions. Feature parameters

would also be useful, but in terms of the core data analysis lies in the deviations of height and its relation to the plane.

2.1.3 Surface roughness measurements

Contact

This form of measurement traces the roughness by physically touching it.

- Stylus profilometer
  The stylus profilometer system is comprised of the stylus. The stylus moves horizontally across the surface and the vertical variation creates an electrical signal which is collected by the detector.

  Landy [5] states that contact roughness measurements are not well suited to the application of ice and snow as the contact would damage these fragile structure.

- Atomic force microscope (AFM)
  This consists of a detector, semiconductor and a cantilever with a probe. This force placed on the material is fed to a piezo scanner which collects the signal. It has an incredibly high resolution but large samples are not suited to this method

- Other methods include the use of a meshboard and a pin profiler

Non-contact

The advantage of non-contact measurements is that they do not interfere with the fragile snow and can be measured from a distance

- Photographing a surface against a background

- Laser profiling

Both laser profiling and photogrammetry can achieve resolutions of less than 1cm. The laser profiler is more suited to measuring areas greater than 1m transects.

Gharechelou conducted a surface roughness profiling experiment with photogrammetry instead of LiDAR [6]. The methodology was able to identify surface roughness for soil and through a derivation find the backscatter coefficient. They used 3 classifications of roughness: less than 2cm, 2cm - 4cm, and greater than 4cm.

Alhasan [7] did experiments with both photogrammetry and LiDAR to compare their findings. It is noted that in the places more surface roughness there was greater variance in results. It is hypothesized that this is due to the shadows presenting noise in the photogrammetry algorithm or the overlapping of different materials in the LiDAR. These experiments were done in the context of measuring surface roughness of roads before and after paving

In 1990, Paterson [8] created a device that measures surface roughness through collecting the RMS height and correlation length. This was done using a camera with flash. These would then be digitized and analyzed to extract the RMS height and correlation length.

These traditional techniques explained above create one dimensional measurements which have limitations. An important aspect is what is described as "anisotropy" which describes the mircostructures of snow. This is where 2D methods have an advantage. Landy mentions the existence of photogrammetry and LiDAR as 2D measurement techniques but that the LiDAR is the more popularized.

2.1.4 LiDAR technology

LiDAR contracted from Light Detection and Ranging. Its functioning is identical to that of the more known RADAR (Radio Detection and Ranging) , but instead of microwave radiation, LiDAR makes use of higher frequencies in the optic region of the spectrum. The smaller wavelength of pulses emitted allows for greater precision

than the traditional radar [3]. LiDAR functions by illuminating a region of space using wave pulses and then measuring the time delay of the reflected signal [9].

2.1.5 Signal processing

Landy assesses that these height deviations are usually assumed to be perpendicular to the reference plane which then allows for good fitting of ordinary least-squares regression. Further research was done to characterize non-linear surfaces by making use of the orthogonal distances. The paper reflects that natural surfaces are rarely able to be characterized by a linear (least-squares) or non-linear (higher polynomial) trends. These cases benefit from the use of a high pass filter based on FFT which eliminates all frequencies below a certain cutoff point.

2.1.6 System Calibration

All LiDAR experiments measuring surface roughness had to make a test scan for calibration. Usually, this consisted of first obtaining a smooth surface which the RMS height can be considered to be zero [5] which would be used to offset the data. Interestingly, Alhasan made use of a 3D printed sphere to do these calibrations [7]. Using this method, the scanner's position to the surface could be monitored and a controlled resolution of the point clouds can be seen. Additionally, a flat target with adjacent tiles of black and white were measured for the same calibration purposes.This paper makes the suggestion that even more calibration and standardization would improve the experiment.

2.1.7 Sea Ice findings

Hong [10] described the relationship between sea ice extent. roughness and refractive index. It describes that a decrease in sea ice extent, decreases the average

surface roughness and increases the average refractive index. The study made use of the Hong approximation. The paper centers on how roughness and refractive index of sea ice relates to its sea ice cover.

Work has been done using LiDAR to measure movement of glaciers [11]. Tellig made use of aerial LiDAR data collected by NASA of glacial areas. The point clouds had a density of one point per $2.7m^2$. The techniques used centred on Particle Image Velocimetry (PIV) which made use of surface roughness and surface feature shapes.

Nolin [12] explored roughness using angular reflectance measurements from the Multi-angle Imaging SpectroRadiometer (MISR) and LiDAR-based roughness measurements from the Airborne Topographic Mapper (ATM). The MISR is satellite based whereas the ATM's measurements are collected from a plane that flies overhead. MISR measurements are limited to weather conditions as they cannot record data is there are clouds overhead. The study found that the roughness variance was greater in the ATM as compared to the MISR.

2.1.8 Land surveying research

Brukbar used LiDAR technology to map microtopography of a region [13]. The study used two datasets: one with a point density of 0.714 points/m2 spacing and another with 10.28 points/m2. Brubaker [13] found in a comparison between two LiDAR datasets that a higher resolution did not improve roughness characterization.They concluded that the algorithm and methodology had a larger effect than the point density.

Bryant did analysis on an abandoned gravel pit, row crop/forest, range/wheat and a cultivated almonds/vineyards [14]. Their experiments concluded that for a

consistent RMS height value of an area ranging from 3.5m2 - 1225m2, at least 20 3m transect measurements.It has also been used to determine soil moisture [15] which lends itself to agricultural applications.

The surface roughness of the pumice plain deposits at Mount St Helen were analyzed by Whelley [16].The research collected here allows for characterization of remote areas and other planets in the solar system.

2.1.9 Engineering products

In addition to landscape analysis, surface roughness is used for a variety of purposes in the commercial engineering world. Tonietto provides analysis of surface roughness of bricks [17]. Roughness lends itself to a variety of applications and there is an established standardization (ISO 25178) which defines these finishes.

2.1.10 Ice characteristics

Parkinson explores the technicalities of ice formation in the Southern Ocean [18]. It analyzes the sea ice extent and thickness in relation to increased CO2 levels.

Peck gives a comprehensive look at the relevance of Antarctic research in the 21st century [19]. It encourages the understanding of ice formation patterns and particularly warns that a rapidly changing Antarctic could be catastrophic for the environment.

2.2 Suggested Approach

2.2.1 Introduction

This section will detail how the material gathered in the literature review relates to the scope of this research project. The insights gained from the studied research will allow for more informed decisions with regards to the methodology and design. It is of paramount importance that experiments are designed with the knowledge obtained in modern literature.

2.2.2 Data collection

The piece of literature most akin to the research objectives is the research by Landy [5]. Although this project does not involve measurements of sea ice.

The literature has shown the need for contact-less surface roughness measurement, especially when applied to fragile ice samples, further motivated the use of LiDAR.

2.2.3 LiDAR type

Although experiments and analysis can be done on collected satellite data, the experiment application of analyzing the "centimeter level" surface roughness would be more suited to shorter range LiDAR such as the Velodyne VLP-16. The VLP-16 only has an accuracy of 30mm, which is quite large considering the roughness magnitudes of sea ice. Ideally, a device with greater accuracy at the small scale should be used, but this can be accounted for by increasing the scale of the surface.

2.2.4 Extrinsic calibration

The method explored by some of the literature of scanning surfaces of known dimensions to provide should be used. It suits this research goal of showing how well the LiDAR can characterize a surface.

2.2.5 Ground truth

Most investigations into the calibration of LiDAR devices involves using planes. As the literature suggests, the plane shape has the advantage that it is easily characterizable by a linear equation and it is a shape that is commonly found in the environment such as a wall or a board. This shape can be useful in determining a ground truth reference level from where the measurements are taken.

2.2.6 Plane characterization

There are multiple mathematical functions to determine a plane fitting, but all use some form of linear regression. The most promising methods found in the research are the use of RANSAC and ICP functions which provide a more robust approach to linearizing a point cloud region. Since point cloud data may contain many points of noise and outliers, this methodology ensures that extreme do not have as great of an effect on model. This is further explored in the Design section.

2.2.7 Suggested shapes

In terms of shapes, the literature shows the use of planes/linear shapes, spherical shapes, pyramidal shapes and other non-uniform shapes. Considering the theory of reflectivity discussed, an uneven surface may cause interference leading to a poor representation of the spatial properties of the object in the resulting point cloud. Although modern LiDAR devices can account for these interferences by using many

laser beams instead of only one, the effect of different known shapes should be investigated. This is where the value of kurtosis and skewness measurements are of use as they indicate how smooth or spiked the surface is.

2.2.8 Surface material choice

Given the complex nature of the reflectivity of ice, this initial investigation should be limited to using surfaces with a uniform reflectivity. Once the general height characterization can be done, then the effect of reflectivity should be investigated.

2.2.9 Surface roughness parameters

The parameters that would be best suited to this characterization is the RMS height, arithmetic height, kurtosis and skewness. This can be calculated on the entire 2D as well as on profiles of the 1D surface.

2.2.10 Conclusion of approach

The literature has allowed an informed decision to be made regarding how the experiment is conducted. It will use the RANSAC algorithm for plane fitting and the ICP algorithm for positional comparison. The material used will be that of a constant reflectivity. Only after the analysis of uniform reflectivity, can experiments be done with ice which has a variable reflectivity.

Chapter 3

Methodology

3.1 Methodology

The experiment focuses on the outputs obtained from LiDAR scans of surfaces with known roughness properties.

The overall methodology explored consists of three main phases: surface design, data collection from the LiDAR scans and data processing as shown in the figure below.

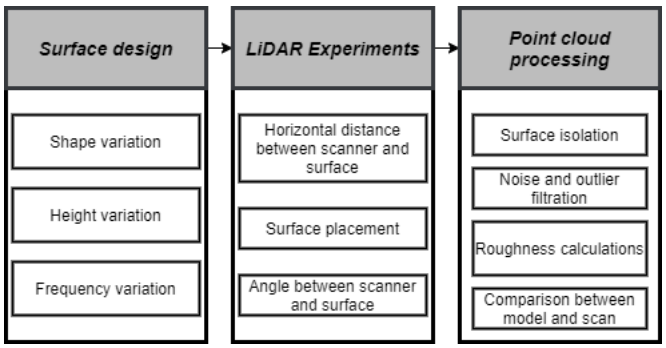

Figure 3.1: Methodology overview

3.1.1 Surface design

This phase involves the creation of known surfaces using Computer Aided Design software. The main variables of the surface are its shape, height, and frequency of the shape resulting in a pattern. A set of surfaces with ranging height, shape and frequency are generated for the purposes of drawing conclusions on the LiDAR's ability to characterize the surfaces.

3.1.2 LiDAR Experiments

This phase involves the experimental set up of the LiDAR in relation to the surfaces. The goal of varying these setup conditions is to develop a methodology that would yield the best characterization of the surfaces. These variables are the horizontal distance between the surface and the scanner, the placement of the surfaces on a flat surface to act as a ground truth and the angle at which the scan is taken. These conditions are varied by maneuvering the Husky Robot to marked points.

3.1.3 Point cloud processing

The output of the LiDAR scans are in a point cloud format. This phase involves the creation of a pipeline which isolates the region of interest by manual cropping, removing outliers and noise, and mapping to a more appropriate coordinate system to obtain the readings relevant to the individual surface scans. Once the surface scan is quantified, the position readings are used to calculate surface roughness parameters. The scanned surface is then compared to the model, ultimately showing the quality of characterization.

Chapter 4

Design

4.1 Introduction

This section will detail the preliminary and final design of the experiment. The preliminary experiments involved only three tiles and a variation in horizontal distance whereas the final experiments used eight tiles, with adjustments in the set up from the preliminary design.

4.2 General experiment rig design

4.2.1 Board

A 6mm thick piece of hardboard was used as a ground truth plane. The hardboard was selected due to its rigidity therefore minimizing a change in the plane throughout the experiments. 100 x 100 mm 3D printed tiles were attached to this board using Prestik. A detailed analysis of the surface design is explained in the next section.

4.2.2 VLP-16 and Husky UGV

The scanner used was a Velodyne VLP-16 that had been fixed to the Husky Unmanned Ground Vehicle. Throughout tests the board kept fixed against a work-bench and the variation in distance between the scanner and the board were done using the Husky's controls. The Husky's movement was controlled using a wireless Logitech gamepad. Holding down the L1 button and moving the left analogue stick would result in the movement of the wheels in the specified direction. The relative position between the board and scanner was changed by moving the Husky with these controls. The data captured by the Husky is collected using an Ethernet cable attached to a laptop. This data is outputted in the form of a rosbag file. A detailed inspection of the files can be found in the point cloud processing section.

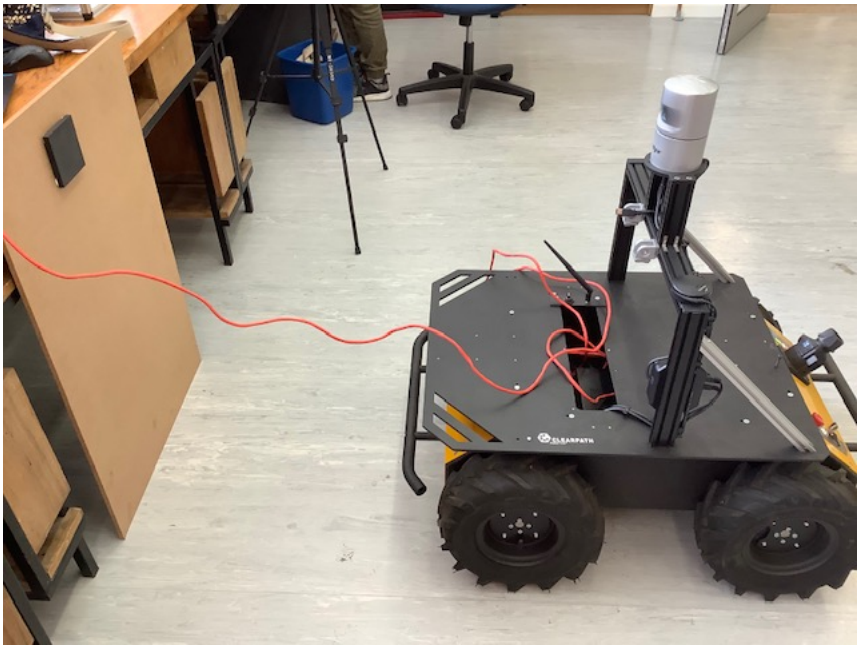

Figure 4.1: Experimental set up showing the relative positioning of the hardboard ground truth with a 100mm x 100mm x 10mm 3D printed rectangle, relative to the Clearpath Husky UGV. The VLP-16 LiDAR is the cylindrical silver object that is fixed to the UGV. An Ethernet cable (shown in red) connects the Husky to the laptop being used to capture the rosbag data.

4.3 Surface Tile Design

4.3.1 Introduction

This section details the design choices of the surfaces with varying roughness used for the LiDAR scans.

4.3.2 Choice of material

For the purposes of this experiment, it was of paramount importance that the surface properties of the designs were known. This experiment focuses on the comparison between the known extrinsic properties of the material compared to the LiDAR point cloud scan of the material, therefore the reference surface should be well characterized. To facilitate this precision required, it was decided design the surfaces in CAD software (AutoDesk Fusion360) which could then be exported to 3D print. In addition to providing greater precision, the surface model can be exported in the form of a point cloud which can be compared to the LiDAR scan's point cloud.

3D printing

The the following 3D printer technologies were explored: [**?**]

- **Fused Deposition Modeling (FDM)**
  Extrudes molten plastic filament from a nozzle layer by layer
- **Selective Laser Sintering (SLS)**
  Uses a high powered laser to fuse particles of polymer powder.
- **Stereolithography (SLA)**
  Uses photopolymerization which cures portions of the resin layer by layer using UV light

Table 4.1: Comparison of Fused Deposition Modelling (FDM), Stereolithography (SLA), and Selective Laser Sintering (SLS) 3D printing technology

	FDM	**SLA**	**SLS**
Material	Thermoplastic filament	Light curing resin	Polymer powder
Precision	Low	Medium	High
Max XY Resolution	0.25 mm	0.05 mm	0.08 mm
Min Layer Resolution	0.1 mm	0.05 mm	0.06 mm
Speed	Fast	Medium	Slow
Cost	Medium - Low	High	Medium

Considering RMS height of micro and meso surface roughness is quite small, initially the goal was to maximise precision. The SLA and SLS have the greatest precision, but they perform at slower speeds than the FDM and are more costly. This means that the experiment would be limited in terms of the number of surfaces that could be printed. Although the FDM printers have a lower precision, the VLP-16 LiDAR only has an accuracy of 30 mm meaning very fine roughness would not be detected by the scanner.

It was thus decided that the FDM 3D printing was best suited to this application. This allows for quality surfaces for the experiments to be printed with minimal costs at a rapid speed.

Prusa Mini

Of the printers using FDM technology, the Prusa MINI was chosen for this experiment. The University of Cape Town has in its possession a total of six Prusa MINI printers.

Table 4.2: Specifications extracted from the Prusa MINI 3D printer datasheet

Build volume	18×18×18 cm
Layer height	0.05 – 0.25 mm with 0.4 mm nozzle
Max speed	200+ mm/s
Filament diameter	1.75 mm
Materials	PLA, PETG, ASA, ABS, Flex

Constraints applied to design

Using the Prusa MINI enforced the following constraints on the surface design process:

- **Build volume**

  Considering the limited 18 x 18 cm board, it was decided to constrain the surface samples to have a uniform area of 10 x 10 cm and height values not exceeding 10 cm.

- **Base structure**

  It was decided that each surface tile should have a rectangular base and then the roughness pattern above this area. This would allow for uniform adhesion to the hardboard. Additionally, the patterns chosen should not contain overhangs that would require supports.

- **Material**

  The material available was black PLA filament.

- **Print settings**

  Although the Prusa MINI is able to print layers as small as 0.05mm, it was decided that a universal layer height of 0.25 mm should be applied. It was

decided due to the LiDAR's resolution and the 3D printer's resolution that all design elements should be limited to a 1 mm precision.

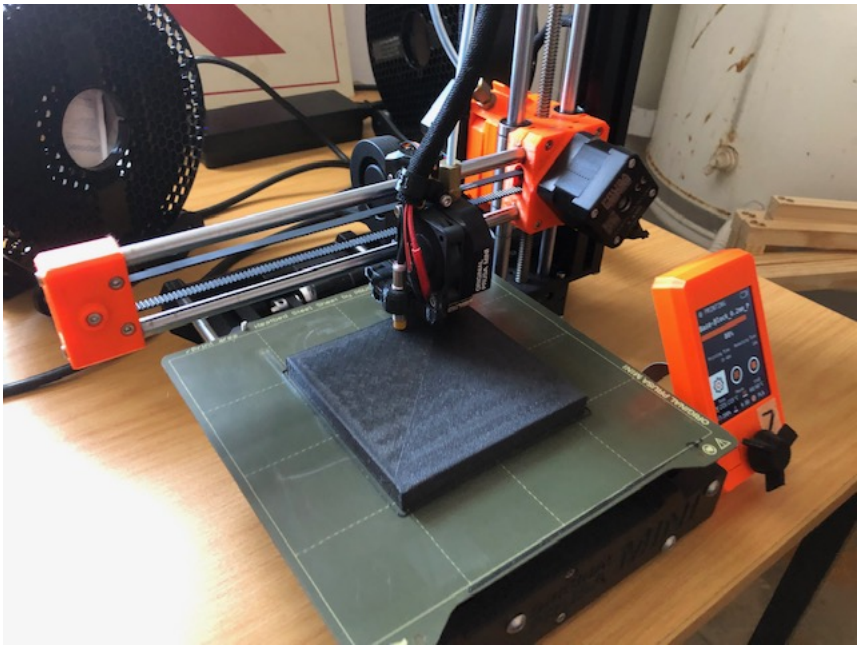

Figure 4.2: Image of the FDM 3D printer, Prusa MINI, in the process of printing a 100 mm x 100 mm surface tile

4.3.3 Shape

Sound proof inspiration

The shape designs were inspired by researching modern sound proofing methods. The objectives of the unusual patterns in the foam, are based on the theory behind sound reflectivity. Similar to the reflectivity of light, sound also exhibits similar dispersion waves when it encounters an uneven surface.

In the practical application of soundproofing, the goal is for the foam surface pattern to disperse the reflection of the sound waves, ensuring sound is reflected

back in many different directions which improves the internal acoustics and limits the sound from transferring out of the room.

Due to the practical application of these surface designs, there is a plethora of industry-lead research into the optimal shape for maximal dispersion.

The shapes found to be most effective and appear in most designs, are pyramids, cones and 3D sinusoidal shapes known as an "egg carton" shape.

These designs are of use to the design pattern of the surface roughness as they provide the optimal shape for dispersion of light which could provide interesting backscatter.

Shape selection

The following general shapes were explored:

- Flat base block
- Pyramid
- Sinusoidal "Egg carton"

Amplitude

Seeing as the estimated accuracy of the VLP-16 is 30 mm, the design amplitudes or heights had to be large enough for the scanner to detect the shape. Although the VLP-16 has this limited accuracy determined by the manufacturer, some papers were able to extract an accuracy value as low as 23mm. Considering the design of the surface is known, height values smaller than this were experimented with.

Frequency

Similarly to the concerns expressed with regards to the height, high frequencies would not register accurately in the scan. The Nyquist sampling theorem states that

in order to accurately reconstruct a signal, the sampling rate should be twice that of the highest frequency.

4.4 Preliminary design and tests

The measurement reference point is shown in the diagram. It is a distinctive ridge marking on the front left bar. The measurement was taken from this point to the point on the board directly opposite this point. The measurements done in this preliminary data collection are in small increments of 10cm except for the closest reading which is taken with the front bar touching the board. At each of the measurement points, each tile is scanned individually as seen in the image on the left and additionally scanned adjacent to one another as seen by the image on the right. Additionally, at the closest measurement where the bar is touching the board, each tile is individually scanned 10cm upwards from its original position and 10cm downwards from its original position.

4.4.1 Tile design

A total of three tiles were designed for the preliminary investigation: a base block which would form as a base for every pattern printed, an egg carton shape with an amplitude of 20mm and a wavelength of 50mm, and a 4x4 pyramid pattern each measing 20mm in height.

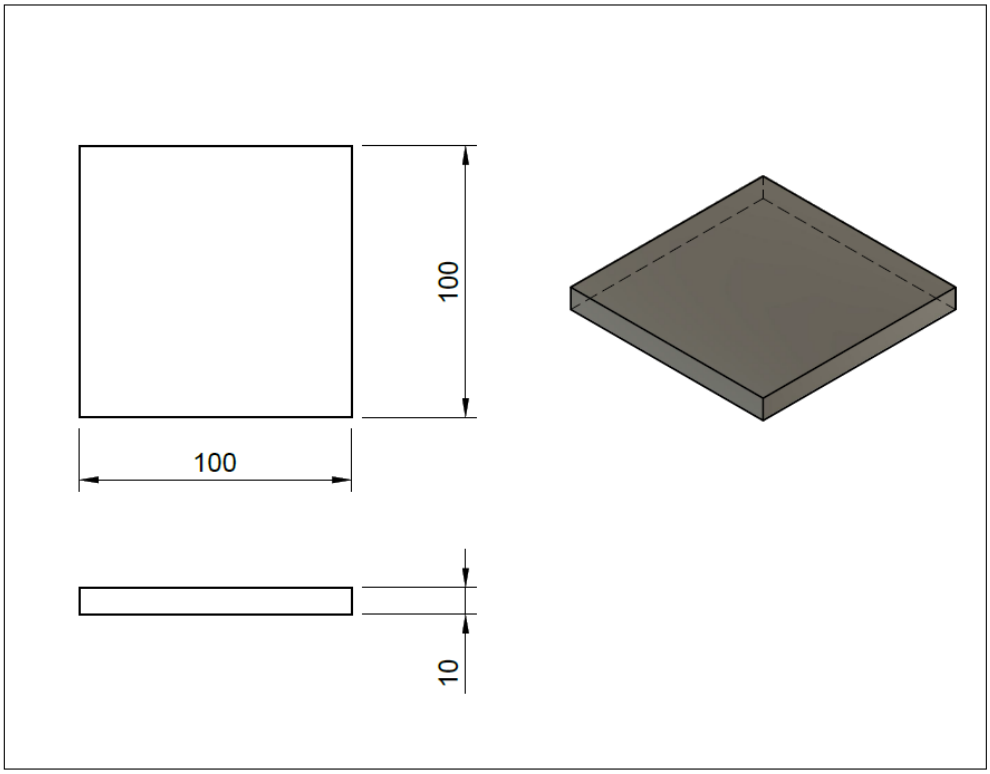

Figure 4.3: Orthographic projection of the base block

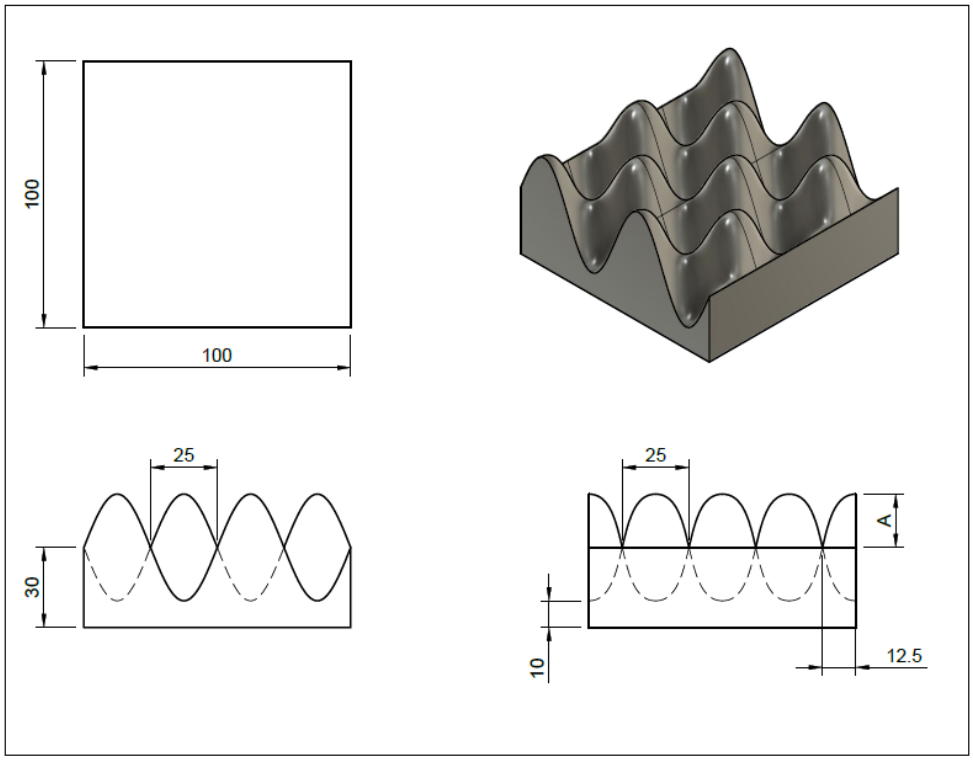

Figure 4.4: Third angle orthographic projection of the egg carton shape. The label A indicates the amplitude.

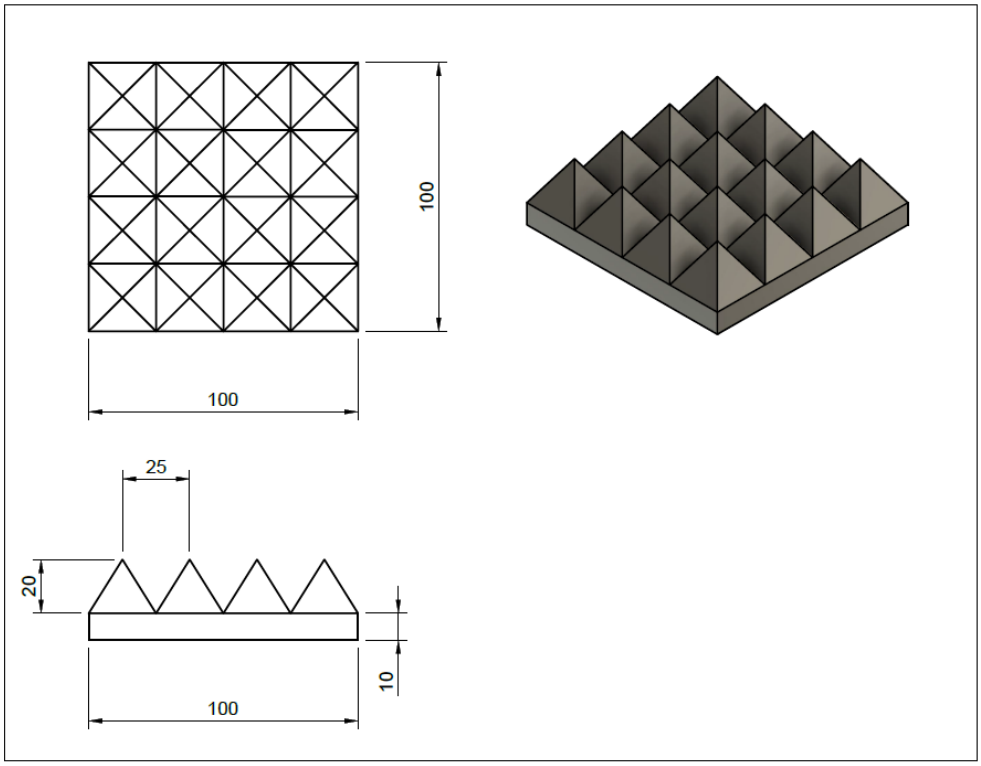

Figure 4.5: Third angle orthographic projection of the 4x4 pyramid shape.

4.4.2 Tile placement

The diagram below shows a mapping system for the tiles on the board which is referred to in the file naming convention.

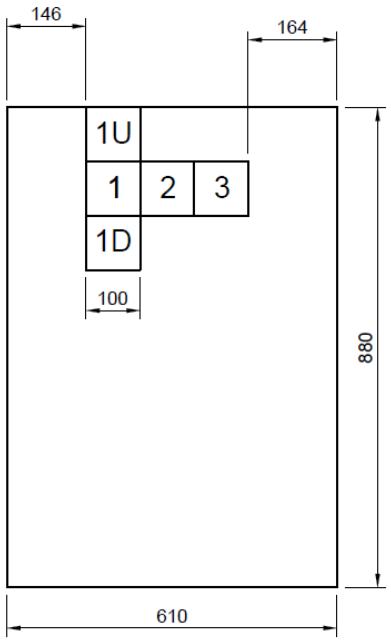

Figure 4.6: The positioning system of the tiles on the board used for the preliminary experiments.

4.4.3 Experiment Description

The measurement reference point is shown in the diagram. It is a distinctive ridge marking on the front left bar. The measurement was taken from this point to the point on the board directly opposite this point.

The measurements done in this preliminary data collection are in small increments of 10cm except for the closest reading which is taken with the front bar touching the board.

At each of the measurement points, each tile is scanned individually in tile position 1 and collectively in positions 1,2,3. Additionally, at the closest measurement where the bar is touching the board, each tile is individually scanned 10cm upwards from its original position (position 1U) and 10cm downwards from its original position (position 1D).

4.4.4 Observations and Recommendations

Upon observing the point clouds, it was evident that the pyramid shape was not very distinctive. All three shapes in one scan compared to individual scans showed no clear signs of distortion or shadows. It was noted that the blocks can be recorded altogether, but that they should be separated a few centimeters to ensure better block separation.

4.5 Final design and tests

4.5.1 Experiment description

The final experiment involved all eight shapes attached to the board. Instead of using the bar intersection reference point, masking take was set up on the floor at varying intervals of 50cm. These masking tape lines were aligned with the axle of the Husky's front left wheel. Additionally, a piece of masking tape was placed in line with the board's intersection with the ground so as to ensure minimal changes in the angle at which the board was positioned. The Husky was fitted with a camera which captured an image of the board at the same time the LiDAR was collecting frames.

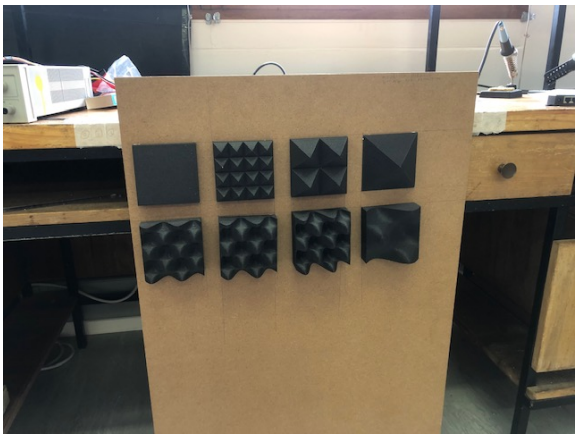

Figure 4.7: Image taken from the final dataset collection

Movement

This session also involved keeping the Husky stationary and moving the board left and right and recording scans. This was done in 1 cm intervals. In addition to taking the stationary scans, a movement from the further left point to the furthest right point was recorded over a number of frames.

Angle

The point on the board perpendicular to the Husky's left wheel was marked at varying angles using masking tape. At these angles, the 50cm marks with masking tape were made. Although these angles were measured precisely using a protractor, it was noted that it was incredibly difficult to align the Husky to the exact angle where the masking tape was placed, hence there is an expectation of some uncertainty in these readings.

Figure 4.8: Image from the final experiment showing the angle markings in masking tape

4.5.2 Tile design

From the preliminary readings, the following shapes were designed which resulted in the final experiment consisting of 8 tiles.

- 2x2 pyramid
- 1 large pyramid
- egg carton half wave length
- egg carton with a larger amplitude
- egg carton with a smaller amplitude

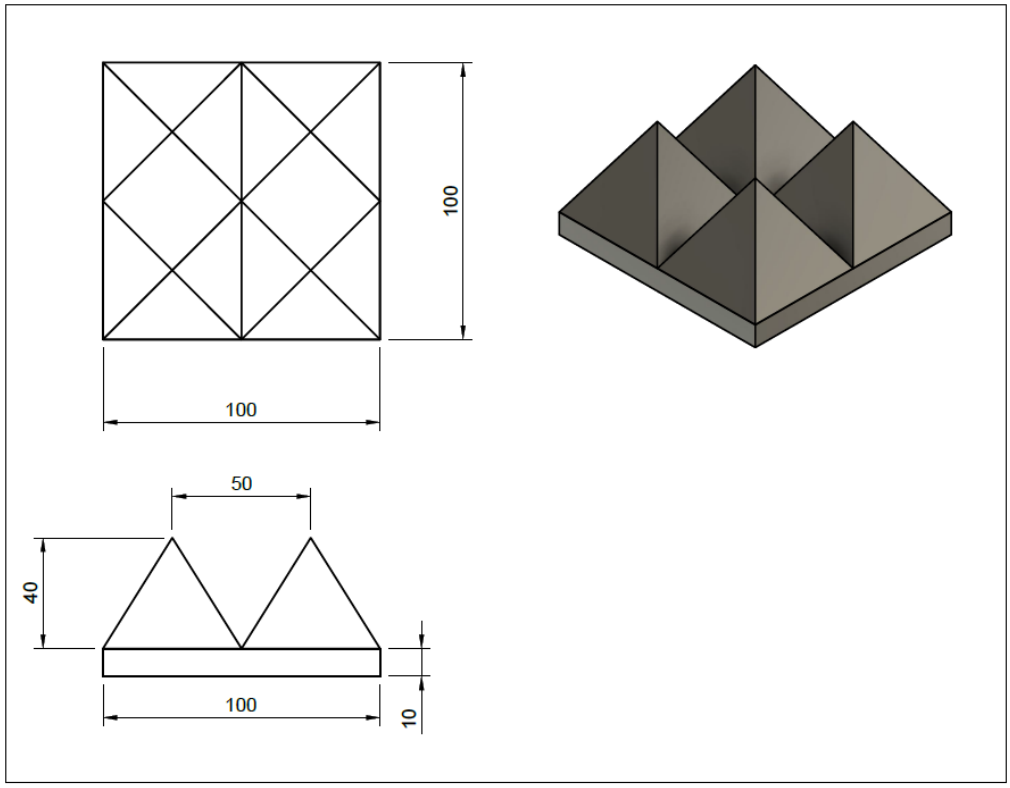

Figure 4.9: Third angle orthographic projection of the 2x2 pyramid shape.

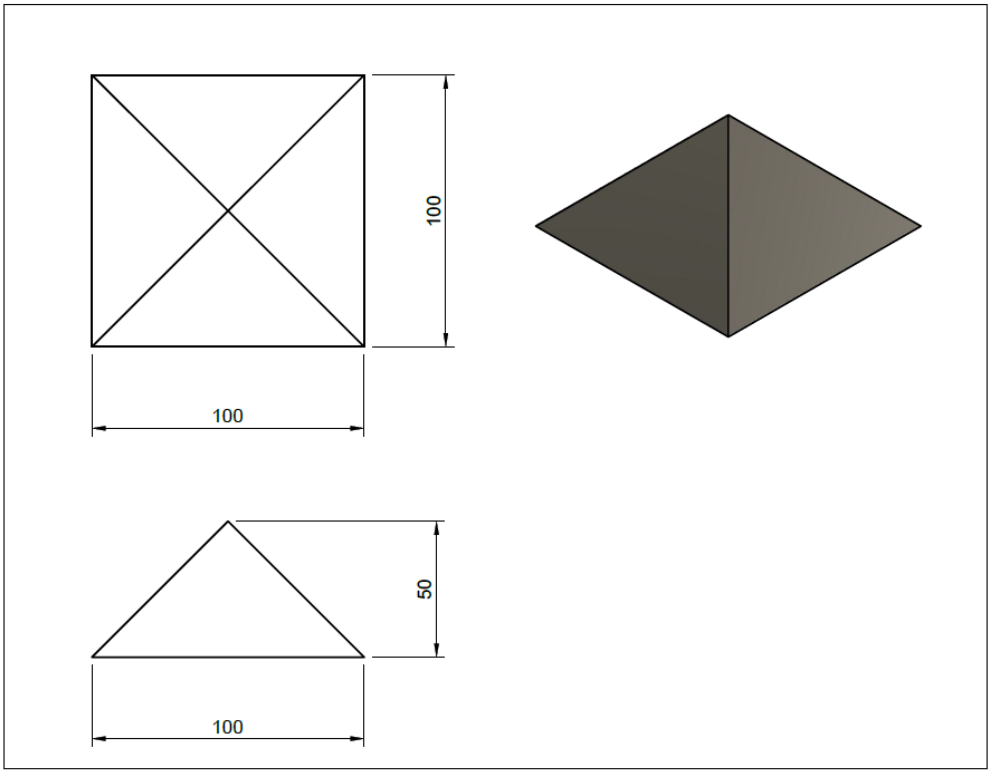

Figure 4.10: Third angle orthographic projection of the large pyramid shape.

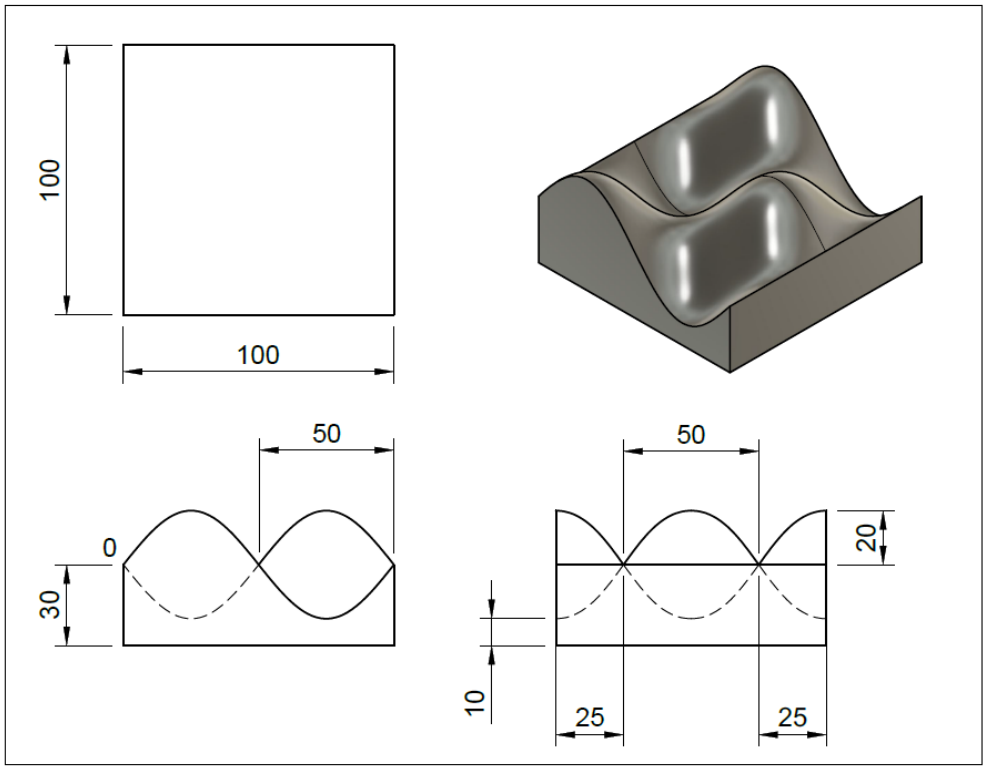

Figure 4.11: Third angle orthographic projection of the egg carton with a longer wavelength.

4.5.3 Tile placement

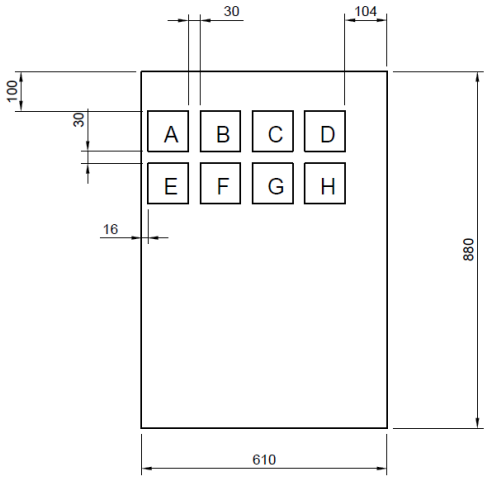

Figure 4.12: The positioning system of the tiles on the board used for the preliminary experiments.

The height, frequency and shape parameters were varied to create unique tiles.

4.6 Point cloud processing

The processing was done in MATLAB due to its point cloud processing functions and compatability with Velodyne LiDARs.

4.6.1 Extraction of point cloud data

The point cloud data captured by the LiDAR comes in the format of a rosbag file. Not only does this contain the information regarding the LiDAR readings but additionally other functionalities of the UGV such as its position and camera readings.

- **Location**

  The pointCloud data structure contains the X,Y and Z locations in meters

- **Limits**

  The XLimits, YLimits and ZLimits contain the maximum and minimumn values for each dimension

1x1 pointCloud

Property	Value
Location	*16x4338x3 single*
Count	69408
XLimits	[-24.2331,6.7038]
YLimits	[-39.0729,10.8979]
ZLimits	[-0.7050,11.3094]
Color	*[ ]*
Normal	*[ ]*
Intensity	*16x4338 uint8*

Figure 4.13: The point cloud object extracted from the rosbag file.

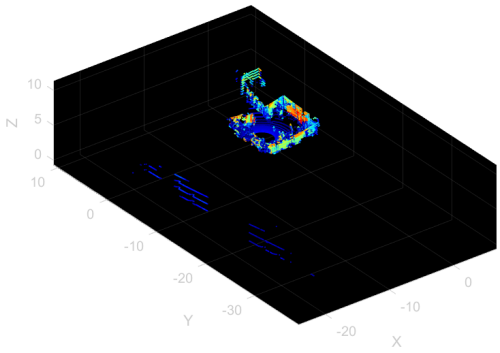

Figure 4.14: The full raw point cloud extracted from the scan

4.6.2 Crop

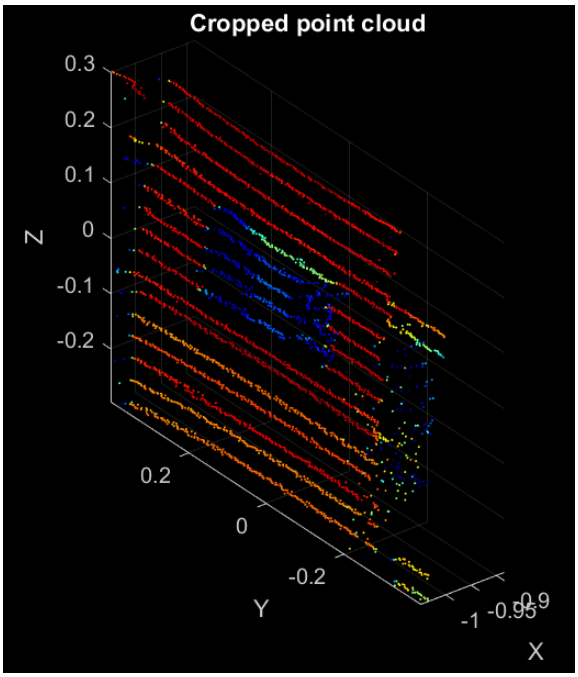

Figure 4.15: The cropped point cloud showing the region of interest

4.6.3 Downsample

Since the VLP-16 consists of multiple spinning lasers, quite often there are overlapping points which can be problematic for data analysis. Downsampling is the process of taking a portion of a larger sample to aid in processing.

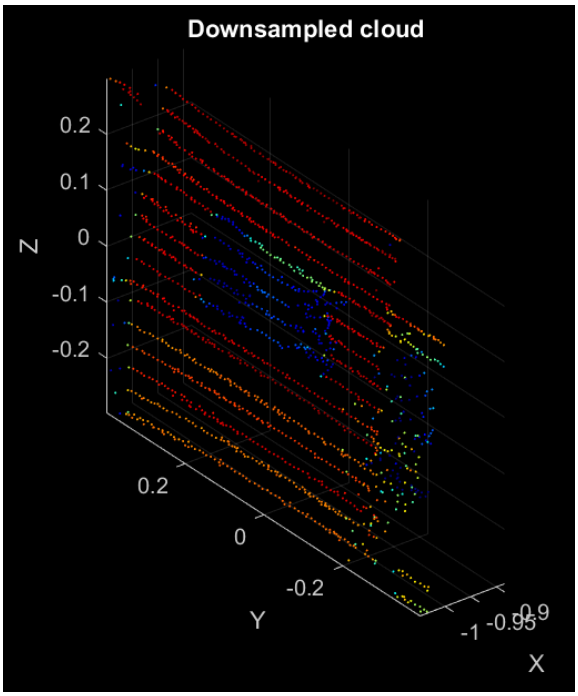

Figure 4.16: The downsampled point cloud

4.6.4 Denoise

The pcdenoise function removes outliers that can be associated with noise,

4.6.5 Separation of tiles and board

Considering the brown hardboard and the black plastic tiles have very different reflectivities, the board and tiles can be separated by reviewing the Intensity property on the point cloud. Any point with an intensity over 60 is determined to be a board point and points with an intensity below this value are considered to be tiles. It is acknowledged that there may be outliers and that the height values should ultimately be the separating factor between the tiles and the board, but for the sake of this proof-of-concept experiment, the intensity separation is proven to be sufficient. Once the separation has taken place, the board points are then matched to a plane using the

RANSAC algorithm. This is expected to have a greater accuracy than plane fitted with the entire point cloud.

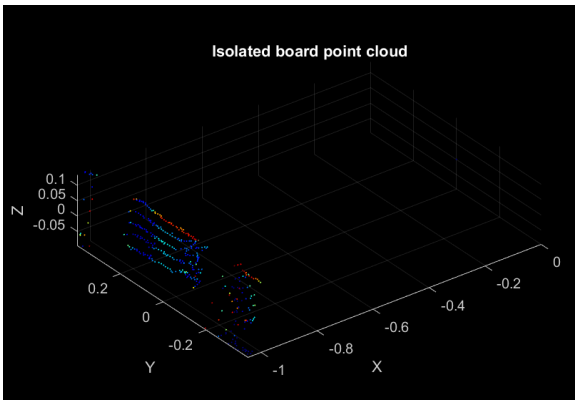

Figure 4.17: Isolated tile point cloud

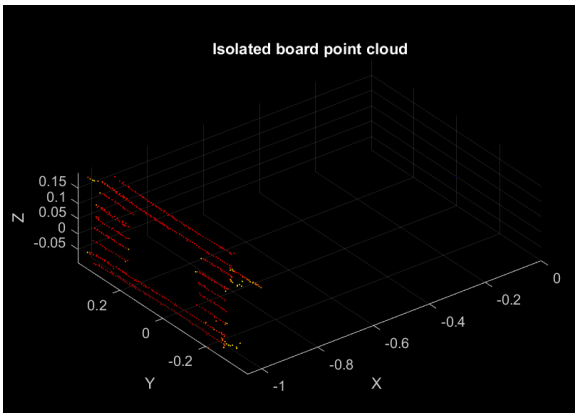

Figure 4.18: Isolated board point cloud

4.6.6 Alignment using ICP

The Iterative Closest Point algorithm is a very useful algorithm for determining the translation and rotation of a point cloud

First principles

Initially, this problem was tackled using first principles. If it is assumed the hardboard is represented by a rigid 2D line and is placed at an angle leaning on a vertical plane which represents the workbench. The goal of the hardboard ground truth is to act as a zero point for the surfaces attached to it and thus the plane must be transformed to this vertical zero point through a rotation to align itself vertically. This can be done by applying a rotation matrix as seen below:

$$\begin{pmatrix} cos\theta & 0 & sin\theta \\ 0 & 1 & 0 \\ -sine\theta & 0 & cos\theta \end{pmatrix} \tag{4.1}$$

Now that the plane is vertical, the height measurement of the surface can easily be done.

This resolves that issue but now a translation of the plane needs to take place to align it with the origin. Since the origin point (0,0,0) of the VLP-16 is located 37.7 mm above the sensor base, it is most likely that the plane would not fall exactly on this line. A translation needs to occur to move the plane to the origin. In addition to converting the data to a more simplified coordinate system, the translation value gives insight into how far away the plane is for the sensor. A translation matrix can be represented like so:

$$\begin{pmatrix} 1 & 0 & 0 & Tx \\ 0 & 1 & 0 & Ty \\ 0 & 0 & 1 & Tz \end{pmatrix} \tag{4.2}$$

The iterative closest point algorithm takes in two inputs: one reference shape and another shape that needs to be moved. It then provides an output in the form of a translation matrix and a rotation matrix.

The movement to the new coordinate system in the first principles method is

unnecessary because once the plane equation is found, the distance between the surface points and the plane can be calculated using this formula:

$$d = \frac{Ax_1 + By_1 + Cz_1 + D}{(A^2 + B^2 + C^2)^{0.5}} \tag{4.3}$$

The goal of using this algorithm to find the rotation and translation matrix is to find the relative positions in space where the boards are. In the experiments, the sensor was placed at various horizontal distances away from the board. These distances were measured using a tape measure, but the LiDAR's scans should reflect the same distances apart in the translation matrix.

ICP implementation

In this experiment, the 50 cm point cloud is taken as a reference and the icp algorithm is applied to each of the other point clouds resulting in a translation matrix and rotation matrix. The translation matrix shows the distance between the two clouds which can be cross checked with the tape measure elements. The rotation matrix is useful for 3D rotations which can be complex to compute from first principles.

Other registration formulae exist but for the purposes of this study, only the ICP is explored.

4.6.7 Robust RANSAC plane fitting

Typically, in linear regression, a line of best fit is constructed which involves finding the equation for the line that best describes the data. This linear regression considers all data points and thus is sensitive to outliers. Often these outliers can be filtered out of the system, but in a point cloud this is often difficult to do. The board was fit to a plane using a method called RANSAC which is used MATLAB's point

cloud processing function pcfitplane. This a robust algorithm that is less sensitive to outliers.

RANSAC pseudocode

- Select 2 random points
- Connect these points using a straight line (y=mx +c)
- For each point calculate the distance between the point and the line
- Repeat K times
- Determine which iteration yielded the largest number of points within a small vicinity of the constructed line

The pcfitplane function returns a model of the plane in the form of a normal vector, a set of inlier indices, a set of outlier indices as well as the root means square error.

Once the plane has been defined, the distance between the plane and each tile point can be calculated using 4.3.

4.6.8 Individual block separation

Separation of tiles into blocks and lines The tile dataset contains a few outliers which are removed manually, The point cloud consisting of eight shapes is then divided into the 8 blocks and then further divided into the number of lines each block has. These individual lines will form part of the 1D surface roughness analysis and essentially gives a profile of a cross section of the object.

4.7 Further processing

This shows the design of further processing to extract the roughness parameters and compare them to that of the orignal model.

4.7.1 Roughness parameter calculations

The RMS, kurtosis, skewness and arithmetic height can be compared once the plane has been aligned to zero. Additionally, with regards to the egg carton and the pyramid, the minimum and maximum values are also of importance.

4.7.2 Comparison between model and scan

Considering the point cloud of the model is available from the Fusion360 stl file, this can be imported into MATLAB and compared to the scans taken.

Pyramid profile analysis

The pyramid can be represented by a piecewise function of linear equations. The model can be mapped to an equation and then the profile extracted from the point cloud can be mapped to can equations. These equations can be compared to assert how well the point cloud maps the shape.

Egg carton profile analysis

The profile's sample rate can be compared to the Nyquist sampling rate. If the sampling rate is less than twice that of the Nyquist sampling rate, this indicates that a quality reconstruction of the wave cannot be completed. A fast fourier transform can be applied to the signal. Once in the frequency domain, high frequency noise can be eliminated using a low pass filter. This filtered data can then be transformed back using an inverse fourier transform.

Chapter 5

Results

5.1 Introduction

5.2 Summary of dataset

The dataset and the code used can be accessed in this GitHub repository: https://github.com/Agi23/LiDAR_FYP. In this repository there is a detailed file naming convention used which identifies which shapes are being measured, what the tile placement looks like and how far away or at what angle this is being measured.

Please find the full dataset's details within the repository. An extract of the preliminary dataset gathered is shown below:

Table 5.1: Subset of the table summarizing the preliminary data gathered. Position refers to the tile placement diagram discussed in the design. The X in the filename represents the distance measured in centimeters. This set was measured at: 14, 24, 34, 44, 54, and 64 cm away from the board using the bar intersection as a reference level

Individual			**Group**		
Shape	**Position**	**Filename**	**Shape**	**Position**	**Filename**
Base	1	X_base.bag	Egg	1	X_base.bag
Egg carton	1	X_egg.bag	Base	2	
4x4 pyramid	1	X_4x4Pyr.bag	4x4 pyramid	3	

5.3 Point cloud analysis

5.3.1 Analysis of ICP calculations

This portion of the results reports on the findings of the pcregistericp function. The 50 cm board was used as a reference cloud and the other boards were compared to this reference. The pcregistericp function produced two transformation matricies: one for the rotation and one for the translation.

The RMS error outputted from this function is summarized in the table below:

Table 5.2: Root mean square error of the ICP algorithm

D (m)	**RMSE (m)**
1	0,03975
1,5	0,03424
2	0,03752

These values coincide with the manufacturer specifications of the VLP-16 have a 30 mm accuracy. The error is constant for all the scans.

Translation

The translation is represented by three values: Δx, Δy, and Δz.

- **Δx analysis**

  The Δx is the change in distance from the scanner to the board. This was expected to follow a linear relationship that would fit to the physical measurements of 100 cm, 150 cm and 200 cm. As shown in the figure below, this relationship was mapped as expected.

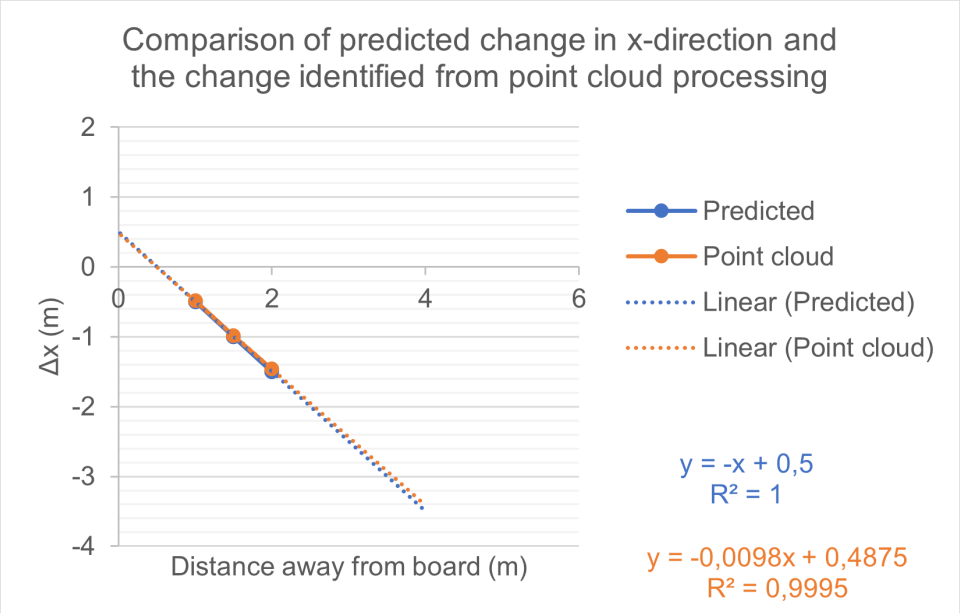

Figure 5.1: The x translation output from the ICP algorithm using the board placed 50 cm away from the scanner as a reference point cloud

The predicted relationship mapped an equation of $y = -x + 0.5$ and the output mapped an equation of $y = -0.0098x + 0.48$ with an R^2 value of 0.9995. This positive correlation suggests a good mapping between the measured values using the tape measure and the values identified by the LiDAR. Although it has such a high R^2 value, this may be misleading because the equation is in

meters. An analysis of the root mean square error shows that the fit has an error of more than 1 cm, which is significant.

The tape measure only has an uncertainty of ±0.05 cm which is significantly smaller than the root mean square error. The additional error could be due to the difficulty associated with aligning centre of the Husky's left front wheel to that of the point marked in masking tape. The masking tape has a width of 1 cm, and the measurement line was recorded at the edge closest to the board, therefore alignment of the axle could not be precisely aligned with this point. For this reason, the RMSE is acceptable regarding the circumstances.

- **Δy analysis**

  The Δy represents the movement of the board left and right. In the experiment, the board is expected to be kept in the same position and the Husky only moves backwards and forwards so hence the Δy is expected to be zero for all the point clouds. The figure below shows that the Δy is in fact non-zero.

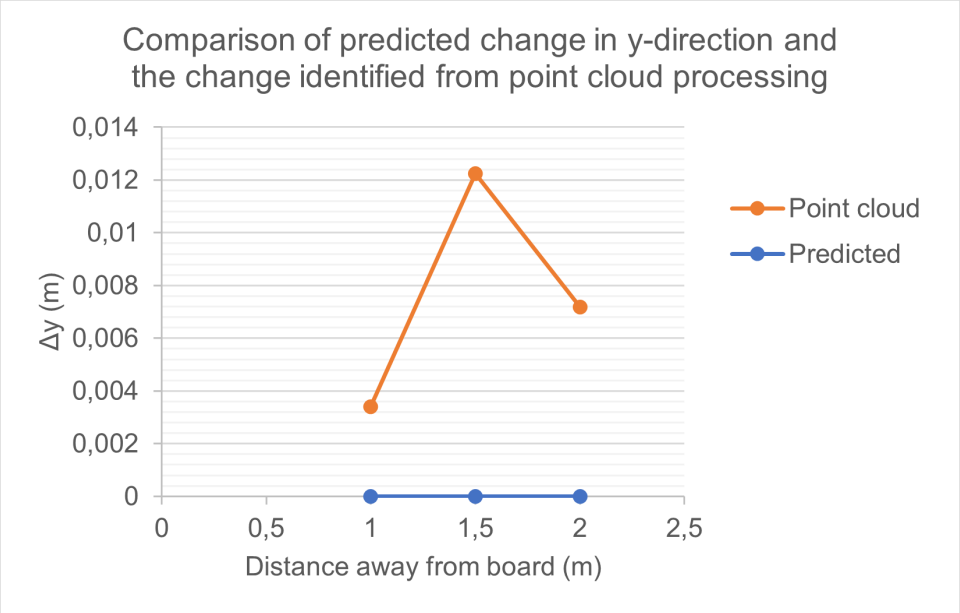

Figure 5.2: The y translation output from the ICP algorithm using the board placed 50 cm away from the scanner as a reference point cloud

Although this graphic may be a cause for concern, looking at the Δy axis, the maximum deviation is 0.012 m and the minimum is 0.004 m. This shows a deviation between 4 mm and 12 mm which is incredibly small. These small deviations could be caused by unintended movement of the board or a movement of the Husky that was exactly perpendicular, but rather at a slight angle. Since the controller's movement is dictated using an analog stick, it is reasonable to assume this angle movement is possible. The analogue stick allows for motion in 360° and thus motion of moving back and forth (90° and 270°) may in fact be a value in the general direction, but not the absolute control. If greater precision in the change of direction is required, the controller should be adjusted to use the arrow keys which would ensure exact perpendicular movement. Generally, this is not strictly necessary as it has a minimal effect in the scans.

- **Δz analysis**

  The Δz represents the change in the boards positioning upwards and downwards. The VLP-16 is in a state of constant motion, allowing it to construct a 360° view of its surrounds horizontal surrounds. The vertical field of vision is limited since there is no rotation around the horizontal axis. As a result of this, the z range is limited to a fixed length and is unable to detail the floor and ceiling of its surrounds. As a result of this relationship, if there is a change in the x direction, the field of vision in the z direction changes. The illustrations below show how this static field of vision is affected by a change in the x axis.

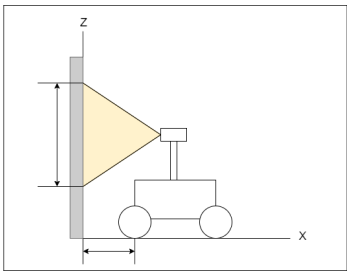

(a) Diagram of the VLP1-16 LiDAR attached to the Husky facing a vertical board (grey). The triangle illuminated in yellow shows the region which will be captured in the point cloud.

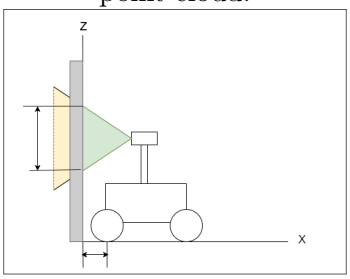

(b) The same view of the experiment as seen in (a), but the distance between the board and the Husky has decreased. The yellow triangle of illumination shown in (a) has been shifted to to the left. The green triangle shows the region which will be captured in the point cloud.

Figure 5.3: A set of illustrations showing the effect changing the distance between the Husky and the board has on the z region captured by the point cloud. It shows that a scan taken closer to the board yields a smaller z area.

This effect explained above is illustrated in the transform generated as there shows a linear change in z when the the distance between the board and the Husky is changed.

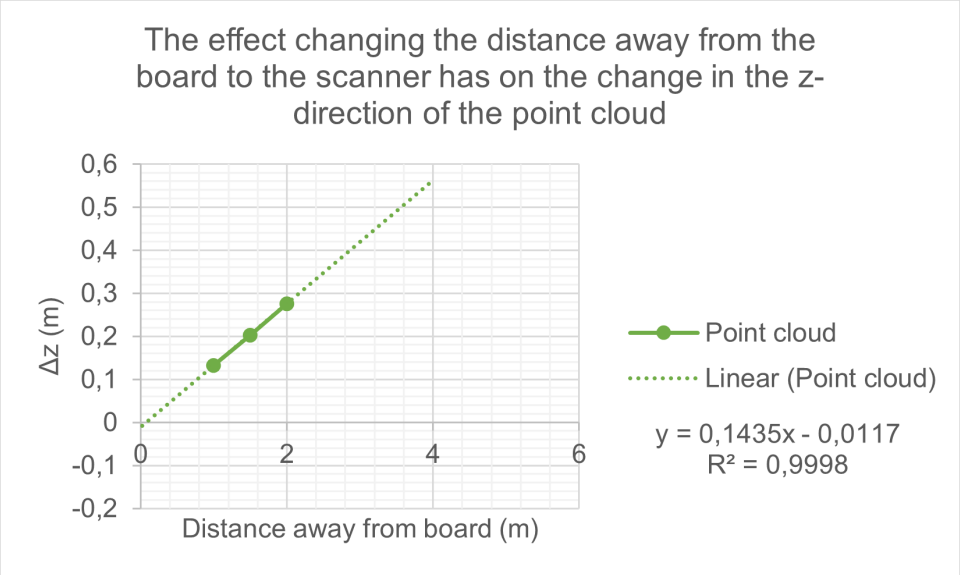

Figure 5.4: The z translation output from the ICP algorithm using the board placed 50 cm away from the scanner as a reference point cloud

5.3.2 Point cloud density

As previously explained, a change in the distance between the Husky and the board has an effect on the region captured in the point cloud. This in turn has an effect on the sampling frequency. A point cloud taken of the experiment board from far away is expected to have fewer points per tile block. The board points are separated from the tile points since the tile points are the points of interest. The figure below shows the number of tile points detected after the separation process.

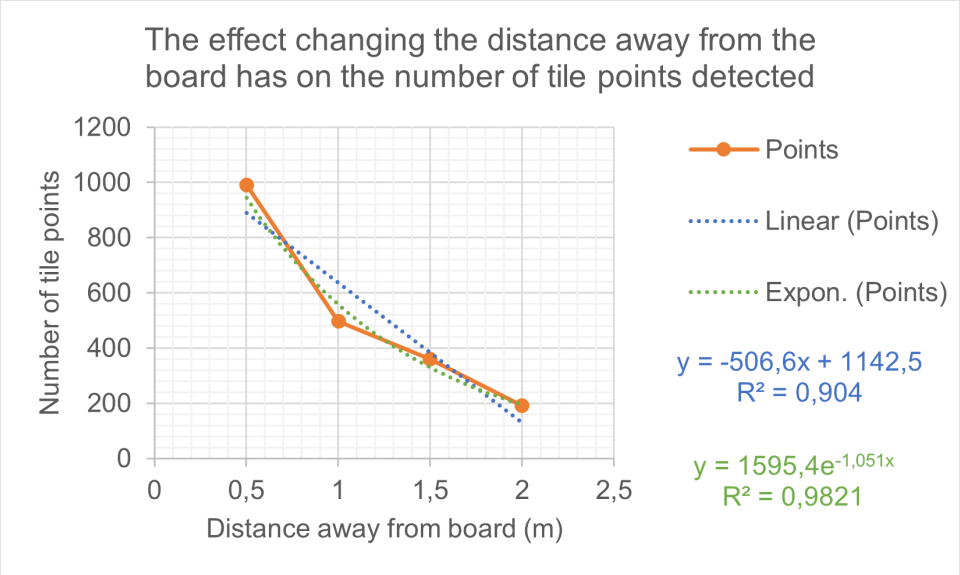

Figure 5.5: Output from algorithm

The graph shows that scans recorded closer to the board yield a greater number of points and hence a larger point cloud density. The trend is exponential and has an R^2 of 0.9821, but it also fits a linear curve with a R^2 of 0.904. Although the exponential does provide a better fit, the most likely conclusion is that the relationship is linear. This is judgement comes from the theoretical understanding of the point clouds. The change between each scan is linear and hence, a linear point cloud density is expected. The reason for these results is due to the small sample size. If further scans are taken in increments of less than 50cm, this relationship can be confirmed.

5.3.3 Plane fitting

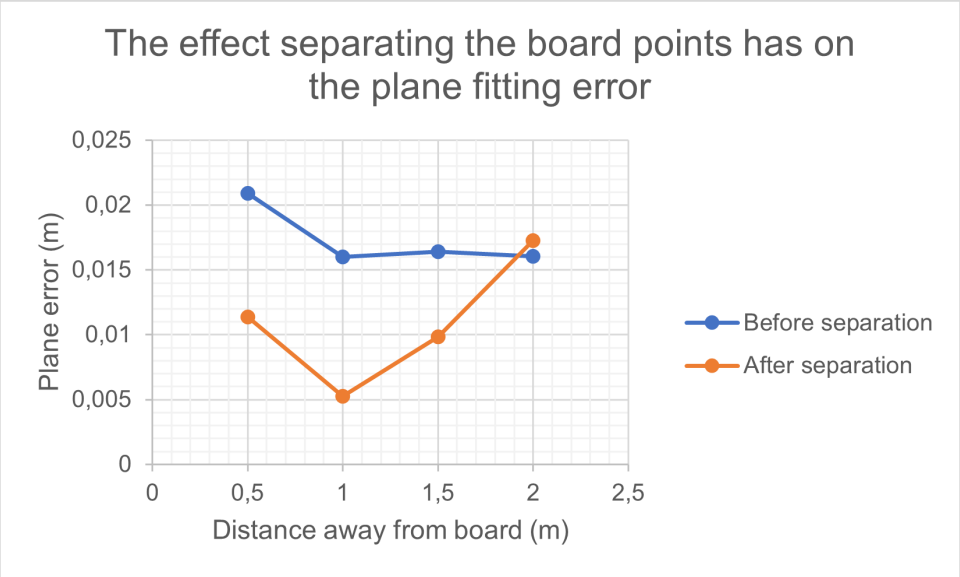

Figure 5.6: This graph illustrates the RMS error of the plane fit. The blue line represents the plane fit error of the whole point cloud (tile points as well as board points) whereas the orange line represents the plane fit performed only using the board points.

Two plane fittings were performed throughout the data process. The initial plane fit used the whole point cloud in the region of interest and then after the separation of tile and board points, the fit was repeated but only with the board points.

Overall, the plane fitting performs better when the tile points are eliminated. The board provides a more uniform surface and hence result in a better fit. The 0.5m to 1m bracket shows a much larger decrease in the plane error from the original plane but this error reduction is not constant. Interestingly, data measured at further distances away had minimal improvements, and the 2m scan even performed worse once the tile points were removed.

This relationship could be due to the point cloud density of the tile points in each scan which was compared in the previous section. The influence surface roughness

has on plane fitting is greatest when there exists a large number of tile points. This height unevenness causes difficulties in the plane fitting, hence why a greater error reduction is seen in the clouds only containing the board points.

Chapter 6

Conclusions

6.1 Conclusions

- A comprehensive dataset was acquired of 8 different tiles of different surface roughness scans taken with varying extrinsic positional parameters. The preliminary tests acquired data at short x direction changes of 10cm whereas the final tests acquired data with 50cm intervals.

- It was found that there was a good position mapping between the scan and measured data by using the ICP algorithm on the point clouds with an overall root mean square error of approximately 3cm which is consistent with the VLP-16's specifications of accuracy. The transform showed a linear relationship in the change in x, a near-zero value for the change in y and a linear relationship in the change in z. A detailed understanding of the positional relationship has been acquired by performing this.

- The translation using the RANSAC method yielded good fits to the point cloud. The application of this plane fitting on the board points separated by intensity, proved to produce a smaller error than that of the whole board including the

tiles.

6.2 Future Work

6.2.1 Analysis of additional data collected

This research mainly focused on the thorough experiment design and data collection. A significantly large amount of data was collected and thus it was not possible to analyze all of this data, but rather a small sample to show proof of concept of the pre-processing. Additional detail not used includes movement, angles, cameras.

6.2.2 Greater point cloud analysis

There are also a great deal of statistical analysis of surface roughness that can be done on this dataset. At its current stage, the existing code is not ready to confidently start defining unknown surfaces. There is some reliance on manual sorting, therefore it would be beneficial to fully automate this process to handle any dataset. This could be done by implementing a more elegant code solution. The detailed analysis of the roughness of the individual objects could not be obtained in the time frame allowed. It is still unknown which roughness parameters are best suited to characterization.

6.2.3 Investigation into the effect of the refractive index of ice

After the model is confident in predicting the surface roughness of known objects, a deeper analysis can be done on the various types of ice floes as demonstrated by [5].

6.2.4 Application to drift models

After the ice has been characterized, this can be incorporated into other models such as those on the UCT Ice Buoy.

Bibliography

[1] R. D. Knight, *Physics for Scientists and Engineers*, 2014.

[2] S. Materials, "crystals The Surface-Roughness E [U+21B5] ects on Light Beam," no. i, 2020.

[3] I. N. Sokolik, "Eas 6145, lecture 14: Principles of active remote sensing: Radar," February 2008.

[4] Keyence, "Introduction to Surface Roughness," 2001.

[5] J. C. Landy, A. S. Komarov, and D. G. Barber, "Secondary-scale surface roughness parameterization using terrestrial LiDAR," *International Geoscience and Remote Sensing Symposium (IGARSS)*, vol. 2015-Novem, no. 3, pp. 2068–2071, 2015.

[6] S. Gharechelou, R. Tateishi, and B. A. Johnson, "A simple method for the parameterization of surface roughness from microwave remote sensing," *Remote Sensing*, vol. 10, no. 11, 2018.

[7] F. Report, "Comparison of Roadway Roughness Derived from LIDAR and SFM 3D Point Clouds," no. October, p. 62, 2015.

[8] J. S. Paterson, B. Brisco, S. Argus, and G. Jones, "In Situ Measurements of Micro-Scale Surface Roughness of Sea Ice Author (s): J . S . Paterson , B .

Brisco , S . Argus and G . Jones Source : Arctic , 1991 , Vol . 44 , Supplement 1 : Remote Sensing of Arctic Environments Published by : Arctic Institute," vol. 44, pp. 140–146, 1991.

[9] F. T. Ulaby, *Fundamentals of applied electromagnetics*. Upper Saddle River, NJ, USA: Prentice-Hall, Inc., 1997.

[10] S. Hong and I. Shin, "Global trends of sea ice: Small-scale roughness and refractive index," *Journal of Climate*, vol. 23, no. 17, pp. 4669–4676, 2010.

[11] J. W. Telling, C. Glennie, A. G. Fountain, and D. C. Finnegan, "Analyzing glacier surface motion using LiDAR data," *Remote Sensing*, vol. 9, no. 3, pp. 1–12, 2017.

[12] A. W. Nolin and E. Mar, "Arctic sea ice surface roughness estimated from multiangular reflectance satellite imagery," *Remote Sensing*, vol. 11, no. 1, pp. 1–12, 2019.

[13] K. M. Brubaker, W. L. Myers, P. J. Drohan, D. A. Miller, and E. W. Boyer, "The use of LiDAR terrain data in characterizing surface roughness and microtopography," *Applied and Environmental Soil Science*, vol. 2013, 2013.

[14] R. Bryant, M. S. Moran, D. P. Thoma, C. D. Holifield Collins, S. Skirvin, M. Rahman, K. Slocum, P. Starks, D. Bosch, and M. P. González Dugo, "Measuring surface roughness height to parameterize radar backscatter models for retrieval of surface soil moisture," *IEEE Geoscience and Remote Sensing Letters*, vol. 4, no. 1, pp. 137–141, 2007.

[15] N. E. Verhoest, H. Lievens, W. Wagner, J. Álvarez-Mozos, M. S. Moran, and F. Mattia, "On the soil roughness parameterization problem in soil moisture retrieval of bare surfaces from synthetic aperture radar," *Sensors*, vol. 8, no. 7, pp. 4213–4248, 2008.

[16] P. L. Whelley, L. S. Glaze, E. S. Calder, and D. J. Harding, "LiDAR-derived surface roughness texture mapping: Application to mount St. Helens pumice plain deposit analysis," *IEEE Transactions on Geoscience and Remote Sensing*, vol. 52, no. 1, pp. 426–438, 2014.

[17] L. Tonietto, L. Gonzaga, M. R. Veronez, C. d. S. Kazmierczak, D. C. M. Arnold, and C. A. da Costa, "New Method for Evaluating Surface Roughness Parameters Acquired by Laser Scanning," *Scientific Reports*, vol. 9, no. 1, pp. 1–16, 2019.

[18] C. L. Parkinson, "Southern Ocean sea ice and its wider linkages: Insights revealed from models and observations," *Antarctic Science*, vol. 16, no. 4, pp. 387–400, 2004.

[19] L. Peck, S. R. Rintoul, M. C. K. Ii, D. Bromwich, D. Liggett, B. Nja, C. Ritz, M. J. Siegert, A. Aitken, C. M. Brooks, J. Cassano, S. Chaturvedi, P. C. Nath, M. N. Raphael, M. Rogan-finnemore, D. M. Schroeder, and L. Talley, "Review Sustained Antarctic Research : A 21 st Century Imperative," pp. 95–113, 2019.

[20] "xkcd: Thesis defense," https://xkcd.com/1403/, (Accessed on 10/20/2017).

[21] "Big bang - warm kitty, soft kitty (sheldon's lullaby sick song) instrumental version lyrics — metrolyrics," http://www.metrolyrics.com/warm-kitty-soft-kitty-sheldons-lullaby-sick-song-instrumental-version-lyrics-big-bang.html?ModPagespeed=noscript, (Accessed on 10/20/2017).

[22] M. Shaw, "Writing good software engineering research papers," in *Software Engineering, 2003. Proceedings. 25th International Conference on*. IEEE, 2003, pp. 726–736.

[23] B. Paltridge, "Thesis and dissertation writing: an examination of published advice and actual practice," *English for Specific Purposes*, vol. 21, no. 2, pp. 125–143, 2002.

[24] U. Eco, *How to write a thesis*. MIT Press, 2015.

[25] I. Graessler, J. Hentze, and T. Bruckmann, "V-models for interdisciplinary systems engineering," in *DS 92: Proceedings of the DESIGN 2018 15th International Design Conference*, 2018, pp. 747–756.

[26] W. Royce, "The Software Lifecycle Model (Waterfall Model)," in *Proceedings of WESTCON*, Aug. 1070.

[27] B. W. Boehm, "A spiral model of software development and enhancement," *Computer*, vol. 21, no. 5, pp. 61–72, May 1988.

[28] J. Taylor and J. G. Hoole, "Robust Protocol for Sending Synchronisation Pulse and RS-232 Communication over Single Low Quality Twisted Pair Cable," in *Proceeding of ICIT*. Taiwan: IEEE, Mar. 2016.

[29] T. Oetiker, H. Partl, I. Hyna, and E. Schlegl, "The Not So Short Introduction to LaTeX 2_ε," https://tobi.oetiker.ch/lshort/lshort.pdf, Jul. 2015, version 5.05.

[30] "IEEE Conference Paper Templates," http://www.ieee.org/conferences_events/conferences/publishing/templates.html.

[31] A. Baboon, B. Charles, D. Ester, and F. Generalson, "An Amazing Title," Their Not-so-awesome University, Technical Report, Apr. 1492.

[32] B. van der Zander, J. Sundermeyer, and T. Hoffmann, "TeXstudio – A LaTeX Editor," https://www.texstudio.org/.

[33] "InkScape Website," http://www.inkscape.org/.

[34] "Voluntary Page and Overlength Article Charges," http://www.ieee.org/advertisement/2012vpcopc.pdf, 2014.

[35] S. Materials, "crystals The Surface-Roughness E [U+21B5] ects on Light Beam," no. i, 2020.

[36] D. Rev, "VLP-16 User Manual," *Velodyne LiDAR, Inc.*, p. 137, 2018.

[37] B. Bhushan, "Surface roughness analysis and measurement techniques," *Modern Tribology Handbook: Volume One: Principles of Tribology*, pp. 49–119, 2000.

Appendix A

A.1 Link to the GitHub

https://github.com/Agi23/LiDAR_FYP

A.2 Ethics approval